RSC Pharmaceutics

ROYAL SOCIETY OF CHEMISTRY

PAPER

View Article Online
View Journal | View Issue

Cite this: *RSC Pharm.*, 2024, **1**, 317

Biocompatible, injectable and self-healable MOF-based anti-freezing eutectogels for higher encapsulation and sustained release of the anticancer drug curcumin†

Nildhara Parsana,[a] Hiral Ukani,[a] Dharmveer Singh Chauhan,[a] Omar El Seoud,[b] Sanjay Mehra,[c] Arvind Kumar,[c] Naina Raje[d] and Naved Malek *[a,b]

Inspired by the antifreeze proteins found in the blood of *Trematomus borchgrevtnki*, a fish from the Antarctic Ocean, herein we developed metal organic framework (MOF) based 'waterless' eutectogels with impermeable nano-domains as antifreeze "soft" materials. The eutectogels were successfully developed through dissolving sodium alginate and ZIF-8, a known MOF, within deep eutectic solvents (DESs) prepared from the environmentally benign biocompatible cryoprotectants glucose and fructose as the HBDs and choline chloride as the HBA. The structural integrity of ZIF-8 and DES was preserved during the eutectogel formation and so also their properties. The eutectogels showcased notable attributes, including antifreeze properties, self-healing capabilities, injectability, adhesiveness, substantial drug loading capacity (~75 000 and ~71 000 fold higher curcumin than in water) and efficient sustained drug release behaviour. Moreover, the eutectogel also demonstrated antibacterial and antioxidant attributes, along with hemocompatibility evidenced by hemolysis levels below 2%. Furthermore, the eutectogel exhibited biocompatibility even at very high concentrations (50 mg mL^{-1}). Leveraging on its robust colloidal forces and an environmentally benign composition, the studied eutectogel proves its suitability not just for pharmaceutical applications but also for high-performance applications that prioritize ecological sustainability.

Received 23rd December 2023,
Accepted 15th March 2024

DOI: 10.1039/d3pm00088e

rsc.li/RSCPharma

1. Introduction

Hydrogels, with superior hydrophilicity, biocompatibility, and customizable viscoelastic properties, are ideal for a range of modern engineering applications. These include drug delivery, flexible electronics, wound dressing, tissue engineering, and soft robotics, among others.[1,2] Due to their water-rich nature resembling biological tissues, hydrogels play a vital role in advanced fields such as drug delivery. However, their water rich composition poses challenges, especially at freezing temperatures. Sub-zero conditions cause hydrogels to freeze, resulting in fragility and loss of flexibility and strength, compromising their efficacy. To mitigate water freezing, conventional approaches such as introducing cryoprotectants (ethylene glycol, glycerol, and dimethyl sulfoxide) into aqueous solutions are followed to substantially lower the freezing point.[3,4] However, there are concerns about the environmental impact and health hazards as a result of the toxicity of these liquids and the tedious process of separating these cryoprotectants after usage. Inspired by the antifreeze proteins (AFPs) present in Antarctic Ocean fish, several synthetic polymers have been developed that show excellent adsorption over an ice surface and hinder ice crystallization and reduce the sizes of ice crystals. For instance, polyvinyl alcohol (PVA) and polyglycerin (PGL) have undergone investigation as substitutes for AFPs.[5] According to a study, trehalose and alginate oligosaccharides have also been shown to significantly improve ice inhibition.[6,7] Another study revealed that introducing PVA into a solution

[a]*Ionic Liquids Research Laboratory, Department of Chemistry, Sardar Vallabhbhai National Institute of Technology, Surat-395007, India. E-mail: navedmalek@chem.svnit.ac.in*
[b]*Institute of Chemistry, University of São Paulo, 05508-000 São Paulo, SP, Brazil*
[c]*Salt and Marine Chemicals Division, CSIR-Central Salt and Marine Chemicals Research Institute, Council of Scientific and Industrial Research, G. B. Marg, Bhavnagar, 364002, India*
[d]*Analytical Chemistry Division, B.A.R.C., Mumbai – 400 085, India*

† Electronic supplementary information (ESI) available: Results pertaining to the characterization of the DES and eutecotgels by FTIR spectroscopy, their mechanical properties using rheology measurements, hemolysis analysis results, and degradation results of curcumin in water as well as of the eutectogels through FTIR spectroscopy. Furthermore, comparative encapsulation efficiency and degradation of curcumin in the studied eutectogels with literature values and kinetic model fitting of curcumin release with the antimicrobial and antioxidant activities of the DESs and their respective gels with and without curcumin. See DOI: https://doi.org/10.1039/d3pm00088e

not only proficiently restrains ice nucleation but also hampers the growth of ice nuclei.[8] Nonetheless, the freezing process tends to lead to the crystallization of a majority of water molecules in the polymer solution, rather than allowing them to remain in a supercooled state below sub-zero temperature.

In contemporary research, new age solvents with exceptional anti-freezing characteristics have surfaced in the scientific literature, and they are labeled as deep eutectic solvents (DESs).[9–13] DESs are a mixture of two or more components: one being a hydrogen bond donor (HBD) and the other a hydrogen bond acceptor (HBA) that form a eutectic mixture with a melting point lower than that of each of the individual components.[14,15] They offer remarkable characteristics such as low viscosity at room temperature,[16] excellent thermal stability,[17] reasonable vapor pressure,[18] and most importantly cost-effective manufacturing[19] along with exceptional anti-freezing characteristics.[9] These exceptional attributes make them valuable in numerous applications, including drug delivery, owing to their adjustable biocompatibility and low-to-nil toxicity. For instance, DES based transdermal drug delivery systems with improved drug (ibuprofen) solubility (7917 times than water) have been recently reported. These DESs when combined with alginate-based hydrogels exhibited improved drug penetration over a 24-hour period, surpassing commercial formulations. This enhancement in solubility and diffusivity was attributed to the synergistic effect of the DESs and alginate.[20] But these DES based hydrogels have limited functionality because of the involvement of water as one of the solvents at freezing temperatures. Circumventing this limitation, DES based eutectogels as drug carriers for the anticancer drug sunitinib malate have been reported. These gels were formed using a choline chloride (ChCl)/ascorbic acid (AA) based natural DES using 2-hydroxyethyl methacrylate (HEMA) as a gelator.[21] Similar to this, 2-hydroxyethylmethacrylate (HEMA) in a NADES of ChCl–fructose was used to develop a pH responsive drug immobilized ion gel for the delivery of the anti-inflammatory drug indomethacin.[22] Likewise, a system using hydroxylated fullerene (TEGs-C60) in a DES (choline chloride/malic acid)–agarose gel was found to have improved elasticity, conductivity, and thermal stability compared to agarose alone. The study also evaluated drug (ibuprofen) release and the antibacterial effects of the gel.[23]

With DESs already showing promise in the biomedical field due to their minimal toxicity, we can take a step forward by combining DESs with metal–organic frameworks (MOFs) to form a hybrid system. MOFs consisting of metal ions or clusters coordinated with organic ligands boast of an exceptionally porous structure and a vast surface area, which enable them to efficiently load drugs with varied polarities.[24,25] By combining eutectogels and MOFs, we aim to develop a highly efficient system that has synergistic advantages such as the unique anti-freezing properties of eutectogels with the superior drug encapsulation capabilities of MOFs, thereby addressing the gap for improved drug delivery performance over a wide temperature window. This novel system holds significant promise, not only in delivering therapeutics but also in diverse fields, where its versatility and efficacy can be maximized even at lower temperatures.

We have embarked on an endeavor to develop nano-vehicles with biocompatible characteristics, such as surfactant-based vesicles,[26,27] coacervates,[28] hydrogels,[29] and MOF-based composites.[30] In this study, we present the development of MOF-based eutectogels with remarkable properties including self-healing, adhesive nature, injectability and, hemocompatibility. The eutectogels were fabricated using choline chloride (ChCl) and glucose (Glu)/fructose (Fru) based DESs. The preparation involved two steps: first, suspending the MOF (ZIF-8) in the DES, and then introducing sodium alginate (SA) to form the eutectogel through intermolecular non-covalent interactions. Scheme 1 shows the structures of the components used in the gel preparation, accompanied by a representative image showing the formed eutectogel. The SA utilized here to form the gel in DESs originates from natural seaweed and is being extensively used in numerous biomedical and pharmaceutical applications due to its biocompatibility and low toxicity.[31,32] Amongst the constituents of DESs, ChCl is a well-recognized HBA, is biodegradable, has low toxicity, and is significantly less expensive,[33] whereas Glu/Fru employed as the HBDs are naturally occurring sugars found in many fruits, vegetables, and other plant-based sources. They are remarkably useful in many different fields, including but not restricted to materials science research.

2. Experimental section

2.1. Materials

Choline chloride (Merck, ≥98.0%), D-fructose (Merck, ≥99.0%), D (+) glucose (TCI, ≥98.0%), sodium alginate (SRL, ≥98.0%), 2-methylimidazole (Merck, ≥99.0%), zinc nitrate hexahydrate (Merck, ≥98.0%) and curcumin (SRL, ≥99.0%) were used as received without further purification.

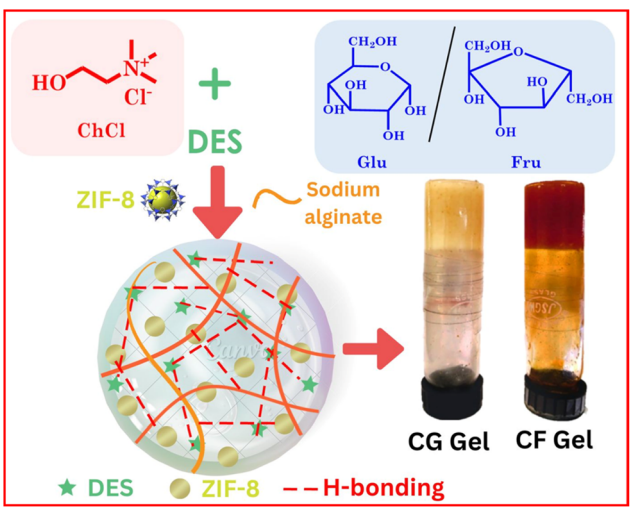

Scheme 1 Structure of the components used in the preparation of eutectogels along with the visual image of the eutectogels.

2.2. Methods

2.2.1. Preparation of DESs. The DESs used in the present investigation were prepared using a reported procedure.[34] Briefly, DESs were prepared using ChCl as the HBA in combination with two HBDs *i.e.*, glucose and fructose in a 2 : 1 ratio and the respective DESs were labeled as CG and CF for Glu and Fru DES respectively. The HBA and HBD were weighed into a suitable beaker and thoroughly mixed with a spatula. With the aid of a magnetic stirrer, they were heated at 60–65 °C until the particles were dissolved and a clear and transparent solution was obtained. Once the components were fully dissolved, the heat source was removed and the mixture was allowed to cool slowly at room temperature. The resultant DESs were hydrophilic and hygroscopic in nature and were stored in a desiccator in the presence of an adsorbent.

2.2.2. Preparation of ZIF-8. In accordance with our previous article,[30] ZIF-8 was prepared using a specific procedure. Briefly, 0.6672 g of Zn $(NO_3)_2{\cdot}6H_2O$ and 12.89 g of 2-MeIm were individually dissolved in 8 mL and 42 mL of deionized water, respectively. The solutions were then stirred at 30 °C for 5 hours before being combined. The resulting solution exhibited a milky turbid appearance. To isolate ZIF-8, the solution was subjected to centrifugation at 10 000 rpm for 10 minutes, resulting in a white precipitate. The precipitate underwent three washes with deionized water, followed by two washes with methanol. Each wash step involved centrifugation at 10 000 rpm for 10 minutes. Finally, the product was dried in a convection oven at 80 °C for 12 hours.

2.2.3. General preparation of eutectogels. Table 1 presents the composition of the components used in this investigation for the preparation of eutectogels. First, the suspension of ZIF-8 in the DESs was prepared before forming the eutectogels. Briefly, a specific amount of ZIF-8 powder was added to the prepared DESs and mixed in a magnetic stirrer to ensure that the ZIF-8 particles were well dispersed throughout the DES. To enhance dispersion further, ultrasonication was employed for 30 min to achieve a better suspension. Following the preparation of the suspension, a certain amount of sodium alginate was added to the mixture, which was then heated at 60 °C in a magnetic stirrer until the particles were dissolved. The mixture was then allowed to cool at room temperature and it formed the eutectogel. A schematic representation of the preparation of the eutectogel is shown in Scheme 2. While examining with various ZIF-8 concentrations, we found that up to 10 mg (1% w/v), ZIF-8 forms a suspension with evenly distributed particles. However, when the concentration goes beyond this point, the particles began to settle, causing an uneven distribution. Thus, we opted for 1% ZIF-8 concentration to achieve an optimal suspension. After considering the suspension with 1% ZIF-8 concentration, we tried different concentrations of SA to study its effect on gel formation and found that at 3% w/v SA concentration, it forms a gel with non-flowing properties. Table S1† shows the effect of different compositions on eutectogel formation.

2.2.4. Fourier transform infrared (FT-IR) spectroscopy. FT-IR spectra of individual components of DESs such as ChCl and related HBDs (Glu and Fru) and their respective DESs were recorded on a Shimadzu FT-IR-8400S spectrophotometer with KBr pellets (1 wt% sample) in the 400–4000 cm^{-1} region. By comparing the FT-IR spectra of the constituent components and their corresponding DESs, it was possible to infer that the

Table 1 Composition of ZIF-8 and the gelator used in the formation of eutectogels in the present investigation

DES (1 ml)	MOF	Gelator	Gel
CF	ZIF-8 (1% w/v)	SA (3% w/v)	CF Gel
CG	ZIF-8 (1% w/v)	SA (3% w/v)	CG Gel

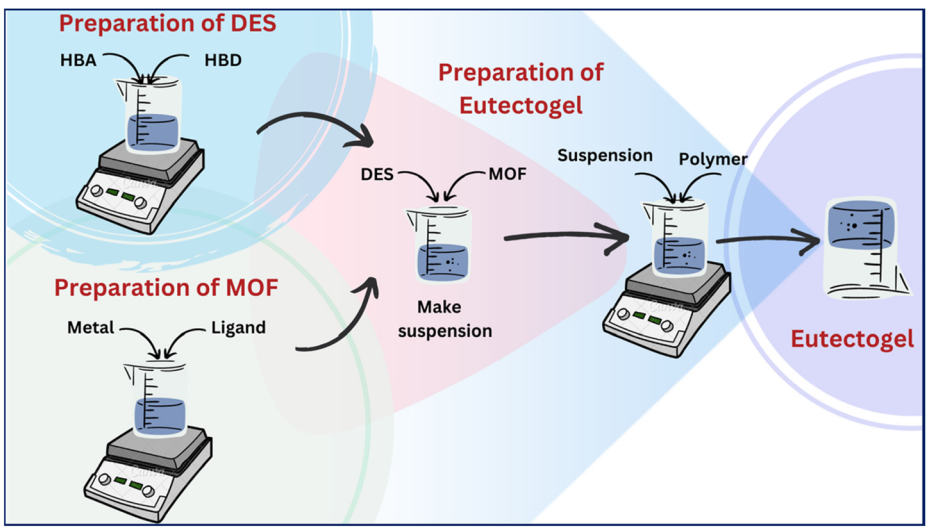

Scheme 2 Schematic representation of the preparation of the eutectogel.

hydrogen bond between the HBD and HBA was responsible for the formation of the DESs. The same method was used to analyse the eutectogels in order to determine any potential interactions that may have contributed to gel formation.

2.2.5. Crystal structure characterization by powder X-ray diffraction (XRD). X-ray measurements were performed using a Philips X'pert MPD system equipped with CuKα radiation (λ = 1.54056 Å) at 40 kV and 30 mA. The measurements covered a 2θ range of 5–50°, with a scanning rate of 3° per minute. This allowed us to analyze the X-ray diffraction (XRD) patterns of both ZIF-8 and the eutectogel, providing valuable insights into their structural characteristics. Furthermore, the signal-to-noise ratio for the eutectogels was determined and found to be 4 : 1.

2.2.6. Scanning electron microscopy (SEM). A Hitachi S-3400N scanning electron microscope with a 15 kV operating voltage was used to capture SEM images of the ZIF-8 powder and eutectogels. Double-sided carbon tape was used to secure the samples to a copper disc once they had dried under ambient temperature. The samples had gold coating on them.

2.2.7. Differential scanning calorimetry (DSC). Differential scanning calorimetry (DSC) was employed on DSC STARe 3 from Mettler Toledo to study the thermal behavior of the eutectogels. The samples were subjected to temperature changes from 20 °C to −140 °C and heated up to 250 °C at a rate of 10 °C per minute, while being continuously purged with nitrogen. Standard aluminum pans were employed, with an empty pan used as a reference and sealed in the same manner as the sample.

2.2.8. Rheology measurements. The rheological properties of the eutectogel were investigated using an Anton Paar MCR 302e rheometer. A plate–plate geometry with a diameter of 49.973 mm and a standard spacing of 0.4 mm was utilized. To maintain a constant strain of 0.5%, frequency scans were conducted within the range of 0.01–100 rad s^{-1}. Strain scans were performed at a fixed frequency of 1 rad s^{-1}, with the strain ranging from 1 to 100%. The rheological measurements were recorded using a strain-controlled rheometer equipped with a Peltier temperature controller and a plate–plate tool.

2.2.9. *In vitro* biocompatibility assay. Hemocompatibility assays were performed on the DESs, ZIF-8, and eutectogels using healthy human blood collected from the Lok Samarpan Blood Bank in Surat, Gujarat, India. The well-established method by Li *et al.* was implemented with minor modifications.[35] The assay involved the centrifugation of blood at 10 000 rpm for 10 minutes, followed by multiple washes in PBS solution with pH 7.4 to separate red blood cells (erythrocytes) from blood. Samples (DESs, ZIF-8 and eutectogels) were prepared at 37 °C in a PBS solution with pH 7.4. Erythrocytes (50 μL) were added to the samples, as well as to negative control (PBS media) and positive control (water). All the mixtures were incubated at 37 °C for 24 hours, followed by centrifugation at 10 000 rpm for 10 minutes. The absorbance of the supernatant was measured at a wavelength of 540 nm using a UV-vis spectrophotometer to determine the rupture of erythrocytes. The hemolysis percentage was subsequently calculated using eqn (1). The experiments were performed in triplicate.

$$\text{Hemolysis}(\%) = \frac{\text{Sample absorbance} - \text{Negative control}}{\text{Positive control} - \text{Negative control}} \times 100 \quad (1)$$

We further assessed the biocompatibility of the studied gels with human keratinocyte (HaCaT) cells using an MTT cell viability assay. HaCaT cells were thawed at 37 °C, from storage at −80 °C. The old cell culture media was replaced with fresh media after centrifugation, and a cell suspension was prepared. This suspension was then transferred to a T-25 culture flask with 5 mL of fresh media and incubated at 37 °C with 4% CO_2 until enough cell growth was achieved. Once a monolayer of cells had formed it was rinsed with PBS and then the monolayer was disrupted by treating it with trypsin–EDTA solution. After 2 minutes, fresh media was added to stop the trypsin's action, and the solution was centrifuged. The suspended cells were mixed with fresh media and transferred to a T-75 culture flask for further growth. Subsequently, these cells were placed in a 96-well plate to evaluate the cytotoxicity of the gels at different concentrations using an MTT assay, and cell viability was assessed by measuring absorbance at 570 nm with a microplate reader after 48 hours.

2.2.10. Curcumin encapsulation within the investigated system. The encapsulation study employed consists of the following steps: initially, acetone, a volatile solvent, was chosen as the medium. Subsequently, a specific quantity of curcumin was added to the acetone based on its solubility (20 mg ml^{-1}). By adding the curcumin solution onto the eutectogel (0.5 g), effective encapsulation of curcumin within the matrix was achieved. The eutectogel acted as a host, absorbing the curcumin particles and securely retaining them within its structure. Upon completion of the encapsulation process, the eutectogel underwent a thorough rinsing with acetone to remove any unbound curcumin, ensuring that only the curcumin encapsulated within the eutectogel matrix remained. A known quantity of the drug loaded eutectogel was collected and subsequently dissolved into a precisely measured volume of methanol. The amount of curcumin loaded within the eutectogel was determined by UV-Vis spectroscopy, involving the comparative assessment of absorbance with the standard calibration curve.

2.2.11. Curcumin release profile and drug release kinetics. Curcumin-loaded eutectogel samples were kept in various PBS solutions, such as PBS 7.4 and 5.0. At predetermined intervals, a sample was withdrawn from each solution and replaced with an equal volume of fresh medium. The curcumin concentration in the collected samples was measured using a UV spectrophotometer at a specific wavelength (λ_{max}) of 431 nm after appropriate dilution. To determine the total amount of released curcumin, a calibration curve for curcumin was employed. This enabled an accurate quantification of the released drug throughout the experiment.

To understand the release mechanism of curcumin from the eutectogel, various kinetic models were employed. These

models included zero-order, first-order, Higuchi, Hixcon-Crowell and Korsmeyer kinetic model. This comprehensive evaluation aimed to determine the precise mechanism underlying the release of curcumin from the eutectogel. For the modeling and comparison of drug release profiles, an add-in program for Microsoft Excel was utilized. This software tool facilitated data analysis and provided a comprehensive understanding of the release behavior of curcumin from the formed eutectogel.

2.2.12. Antibacterial activities. All systems, including DESs and their corresponding gels with or without curcumin, were assessed for antibacterial activity against pathogenic Gram-positive bacteria (*Bacillus subtilis*, *Staphylococcus aureus*) and Gram-negative bacteria (*Salmonella typhi*, *Escherichia coli*) using the qualitative agar disc diffusion approach. Different agar plates were cultured with distinct pathogens and incubated with a specific concentration of the system under study. The zone of inhibition was assessed after 18–20 hours of incubation at 37 °C. The experiments were conducted in triplicate.

2.2.13. Antioxidant activities. The DPPH radical scavenging activity assessment was performed in compliance with the established methodology outlined in the literature.[36,37] The reaction system consisted of 0.5 mL of samples (CG DES, CF DES, CG Gel, CF Gel, CG Gel + Cur, and CF Gel + Cur), 3 mL of methanol, and 0.3 mL of 0.5 mM 2,2-diphenyl-1-picrylhydrazyl (DPPH) radical solution in methanol. After incubation for 45 minutes, the absorbance was measured at 517 nm using a UV-Vis spectrophotometer. The (%) percentage inhibition was calculated using eqn (2).

$$\%\ \text{inhibition} = [(A_{\text{control}} - A_{\text{sample}})/A_{\text{control}}] \times 100 \qquad (2)$$

where A_{control} is the absorbance of the negative control at the time of solution preparation and A_{sample} is the absorbance of a sample after 45 min.

The time-dependent DPPH scavenging activity was assessed using 0.5 mL of the collected samples from the drug release study at different time intervals (4, 8, 16, 32, and 48 hours). The samples were mixed with 3 mL of methanol and 0.3 mL of DPPH solution and then incubated for 45 minutes, followed by measuring the absorbance at 517 nm using a UV-Vis spectrophotometer. The experiments were conducted in triplicate.

3. Results and discussion

3.1. Characterization of DESs and eutectogels

We utilized FT-IR analysis to examine each DES and compared its spectra to those of its respective individual components (Fig. 1(a) and S1(a)†) to investigate the molecular interaction responsible for DES formation. ChCl spectra revealed distinctive vibrational bands at 3324 cm^{-1}, 1475 cm^{-1}, 1092 cm^{-1}, and 950 cm^{-1}, which are attributed to N–H stretching, C–H bending, C–N stretching, and C–O stretching vibrations, respectively.[38] However in the Glu spectra, peculiar bands at 3354 cm^{-1}, 2939 cm^{-1}, 1432 cm^{-1}, and 1049 cm^{-1} are attributed to O–H stretching, C–H stretching, C–O–H bending, and C–O stretching vibrations, respectively. When ChCl and Glu combine to form a DES, it exhibited combinations of peaks observed at 3318 cm^{-1}, 2917 cm^{-1}, 1476 cm^{-1}, and 1030 cm^{-1}. The O–H vibrational band of glucose at 3354 cm^{-1} widened and shifted to 3318 cm^{-1} in CG DES. Glucose, being rich in hydroxyl groups, acted as a hydrogen bond donor and interacted with Cl^- and the O–H group of ChCl, which acted as hydrogen bond acceptors. This interaction led to the shifting of the OH band in the DES.[38] The formation of hydrogen bonds caused the vibrational bands of CO at 1049 cm^{-1} and CH_2 at 2939 cm^{-1} in glucose to shift to 1030 cm^{-1} and 2917 cm^{-1}, respectively, in CG DES. This shift was a result of the influence of hydrogen bonding interactions on these specific functional groups. Similarly, in CF DES vibrational bands were obtained at 3312 cm^{-1}, 2927 cm^{-1}, 1056 cm^{-1}, 1050 cm^{-1} and 1475 cm^{-1} which are attributed to O–H stretch-

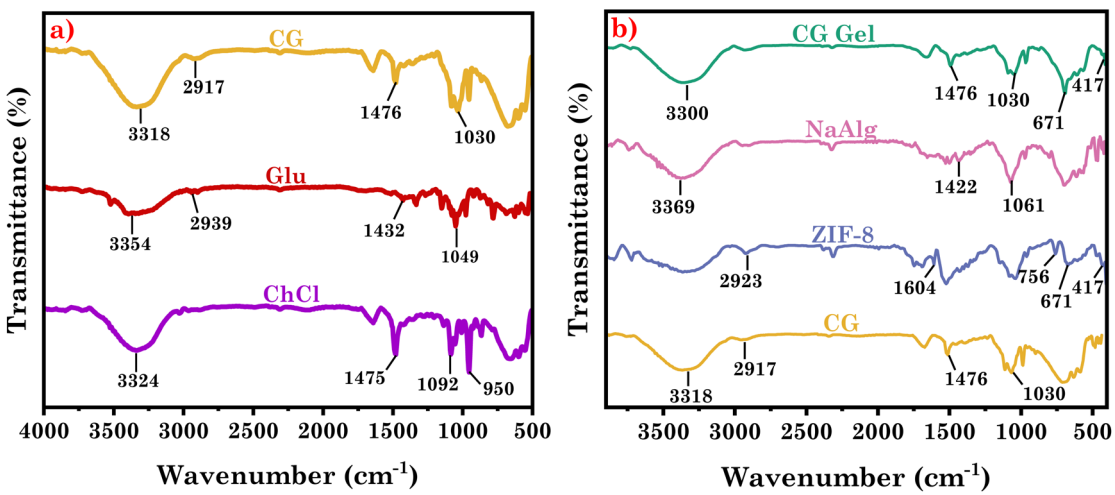

Fig. 1 FT-IR spectra of (a) ChCl, Glu and, CG; (b) CG, SA, ZIF-8, CG Gel.

ing, C–H stretching, C–O stretching (from Fru), C–N stretching (from ChCl), C–H bending (from methyl group of ChCl) respectively. In CF DES, the OH vibrational band of fructose, initially at 3351 cm^{-1}, shifted to 3312 cm^{-1}. This demonstrates that the components established hydrogen bonds to form the DES.[38]

To further investigate the interactions responsible for eutectogel formation, we conducted FT-IR investigations, comparing eutectogel spectra with those of their respective DES and gelator used in gel formation. Also, to validate the existence of ZIF-8 in the formed eutectogel, we conducted FT-IR analysis on ZIF-8 powder and compared the spectra with those of the eutectogel (Fig. 1b and S1b†). SA spectra revealed characteristic vibrational bands at 3369 cm^{-1}, 1061 cm^{-1}, and 1412 cm^{-1}, which are attributed to O–H stretching, C–O stretching, and C–H bending respectively.[39] The FT-IR spectra of ZIF-8, revealed distinctive vibrational bands *i.e.*, a broad band at 3200–3500 cm^{-1}, 2923 cm^{-1}, 1604 cm^{-1}, 756 cm^{-1}, 671 cm^{-1}, and 417 cm^{-1} corresponding to N–H stretching,[40] C–H stretching, C=N stretching (imidazole), C–N bending (imidazole), Zn–O stretching, and Zn–N stretching, respectively.[40] The interaction of DES molecules with the SA in the eutectogel is evident from the –OH stretching frequency of DESs that is shifted from 3318 cm^{-1} (from CG) to 3303 cm^{-1} in CG Gel and 3312 cm^{-1} (from CF) to 3283 cm^{-1} in CF Gel, which suggests the establishment of the hydrogen bond that results in the formation of the eutectogels.[34] The spectra of the eutectogel closely resemble those of the respective DESs, except for specific changes such as the OH band shift due to the interaction of SA with the DES. This suggests that the DES remains intact within the eutectogel structure. Moreover, it is noteworthy that the N–H band in ZIF-8 merges with the O–H band following gel formation. The appearance of distinctive peaks at 671 cm^{-1} and 417 cm^{-1} in both gels, which are attributed to Zn–O and Zn–N coming from ZIF-8, confirms the presence of ZIF-8 in eutectogels, as shown in XRD results *vide infra*.[41,42]

To further confirm the integrity of ZIF-8 within the eutectogels, we performed XRD analysis of neat ZIF-8 and eutectogels (Fig. 2). The prominent diffraction peaks of ZIF-8 are observed at 7.39°, 10.42°, 12.76°, 16.48°, and 18.08°, corresponding to the crystal planes (011), (002), (112), (013), and (222), respectively.[41,42] Remarkably, these diffraction peaks are well preserved in both the eutectogel samples. The XRD peaks of ZIF-8 and eutectogel showed no discernible differences, suggesting that the stable structure of ZIF-8 was maintained even after the formation of the eutectogel. This indicates the robustness and structural integrity of ZIF-8 within the eutectogel framework.[30,41,42]

To investigate the morphology of the prepared ZIF-8 and representative eutectogel (CG Gel), we employed scanning electron microscopy (SEM). Fig. 3a depicts ZIF-8 as individual particles, displaying its dodecahedral shape and size as evident in literature. The surface of ZIF-8 may exhibit a textured appearance, with features that can range from smooth to rough and irregular shapes. Additionally, it provides valuable information about the spatial arrangement and even distribution of ZIF-8 particles.[43] Fig. 3b revealed a three-dimensional (3D) network structure with a rough or textured surface which could be attributed to the presence of suspended ZIF-8 particles in the eutectogel. The SEM image confirms the successful incorporation of ZIF-8 particles into the eutectogel, validating their existence within the gel matrix.[42,43]

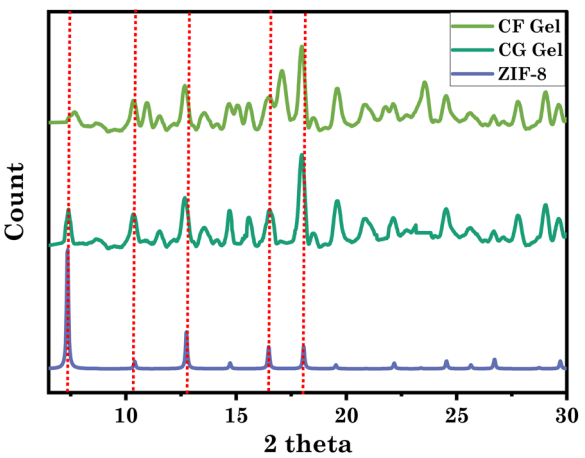

Fig. 2 XRD pattern of ZIF-8 and eutectogels.

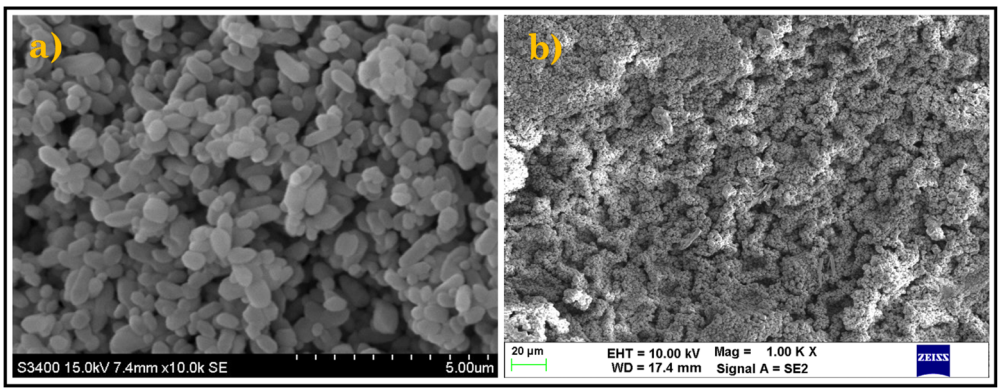

Fig. 3 SEM image of (a) ZIF-8 and (b) representative CG Gel.

3.2. Gel-to-sol transition and freezing behavior of eutectogels

DSC was employed to study the thermal behavior and properties of the eutectogel across a wide temperature range. The results revealed that the gel-to-sol transition temperatures (T_m) were 79 °C for CG Gel and 74 °C for CF Gel (Fig. 4b). Additionally, through rheological analysis, we carried out measurements for the storage (G') and loss (G'') modulus over a temperature range from 25 to 90 °C (Fig. 4c and d). It is noteworthy that the transition from a gel to a sol phase was discernible when the crossover point was detected around 74 °C for CG Gel and ~80 °C for CF Gel. Remarkably, these findings corroborated the DSC data and the observations from manual heating experiments, where the gel exhibited a gel-to-sol transformation within the corresponding temperature range (Video S1†). Furthermore, the freeze-tolerance ability of the eutectogels was assessed through DSC, revealing the freezing temperatures (T_f) of −102 °C for CG Gel and −90 °C for CF Gel as seen in Fig. 4a. Furthermore, in a manual experiment the as-prepared representative eutectogel (CG Gel) was kept in a refriger-

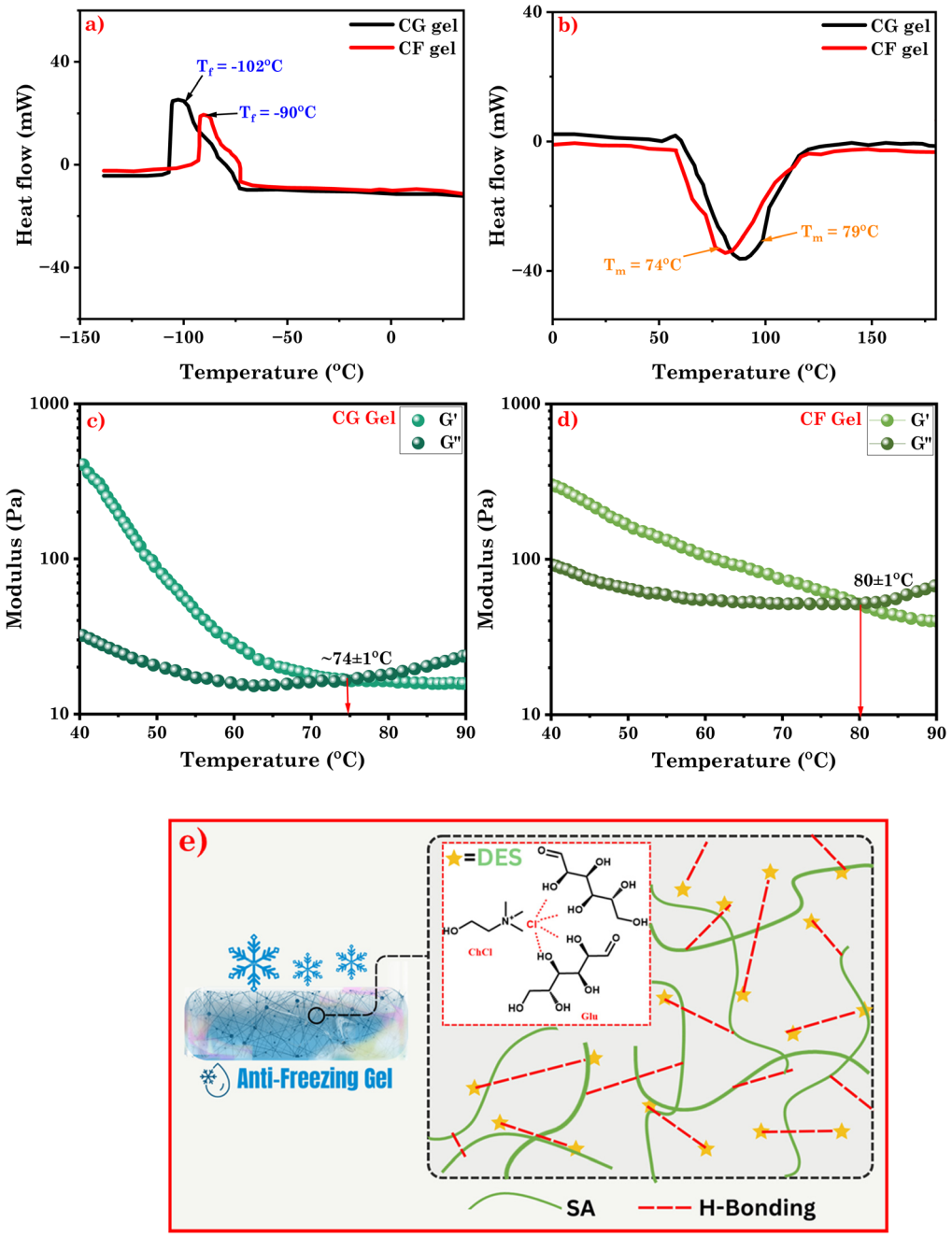

Fig. 4 (a), (b) DSC thermograms of CG Gel and CF Gel; temperature sweep measurement of (c) CG Gel and, (d) CF Gel; (e) schematic representation of mechanism of anti-freezing behavior of eutectogel.

ator (−20 and −50) for 6 hours to observe its anti-freezing behavior. As depicted in Fig. S2,† the eutectogel remained stable without freezing at the specified temperatures, exhibiting no shrinkage or alteration in its physical appearance. These findings highlight the remarkable capability of the eutectogels to withstand extremely low temperatures, further expanding their potential applications. The antifreezing characteristics of eutectogels can be attributed to the DESs used as a solvent in gel formation. DESs exhibit strong intermolecular interactions, primarily through hydrogen bonding between the HBD and HBA components as already shown in FTIR analysis *vide-supra* (Fig. 1). These interactions disrupt the formation of a regular crystalline lattice structure that typically occurs during freezing, thereby preventing the DES from solidifying at lower temperatures.[44] Fig. 4e depicts a schematic representation illustrating the mechanism behind the antifreezing behavior of the eutectogel. Our findings align with prior research on antifreezing characteristics of DES-based systems across various fields.[45–47] However, our study presents a novel approach in the biomedical field by utilizing a composite of DES and MOF with antifreezing capabilities and high encapsulation efficiency for the anticancer drug curcumin.

3.3. Mechanical properties of the eutectogels

We conducted rheological tests to examine the mechanical properties of the eutectogels. The loss modulus (G'') denotes the energy dissipation and viscous behavior, whilst the storage modulus (G') depicts the elasticity and strength of the gel.[29] The G' to G'' ratio offers insights into the mechanical properties of the gel, indicating its softness or stiffness. Herein, we conducted strain- and frequency sweeps as part of the oscillatory rheological measurements for our eutectogels. The linear viscoelastic area for both gel samples were determined using the angular frequency sweep test (Fig. 5b, S3b†). The findings indicate that the eutectogel is elastic at a broad range of frequencies since G' is higher than G'' for both eutectogels up to a wide range of frequencies (up to 100 rad s^{-1} at 0.5% fixed strain).[48]

Furthermore, we conducted strain sweep measurements at a constant angular frequency of 1 rad s^{-1} (Fig. 5a and S3a†). Results showed that both gel samples displayed higher G' values compared to G'' within the linear viscoelastic area, suggesting gel-like behavior.[49] In the case of CG Gel, initially, G' was higher than G'', and these values remained consistent across various frequencies, indicating a linear viscoelastic region with constant elasticity and viscosity. However, as the strain exceeded 4%, a crossover was observed where G'' exceeded G', indicating the breakdown of the gel structure due to disrupted hydrogen bonding. In the case of CF Gel, crossover was observed approximately at 3% strain, suggesting a sligtly less mechanical strength compared to CF Gel. In our previous study, surfactant-based supramolecular eutectogels exhibited lower mechanical strength than the studied eutectogel, *i.e.*, γ_c = 1%.[34] When studied for mechanical strength, the amino acid-based eutectogels revealed G'' surpassing G' as strain exceeded 1% at a constant 1 rad s^{-1} frequency.[48] Similarly, self-assembled eutectogels with DBS (5% w/w) showed weak mechanical behavior, crossing over at approximately 0.5% for the eutectogel.[50] Fracto-eutectogels exhibited 0.3% crossover, transitioning from gel to sol.[51] Collectively, these findings suggest the improved mechanical strength of the investigated eutectogels.

Furthermore, we found that following a significant amplitude oscillatory breakdown, the gel demonstrated rapid recovery, known as thixotropic behavior.[34,52,53] This remarkable ability allows the gel to regain its original structural integrity and mechanical characteristics after breakdown. In both cases, we observed that the G' values of the eutectogels decreased significantly in response to a large-amplitude oscillatory strain (20% strain; 1 rad s^{-1}), causing them to exhibit liquid-like behavior. However, when the strain amplitude was decreased (0.1% strain; 1 rad s^{-1}), the eutectogels quickly regained their quasi-solid state, and G' recovered to its initial values as can be observed in Fig. 5c and S3c.† This ability of the eutectogels to transition between a nearly liquid state and a quasi-solid state highlights their remarkable responsiveness to changes in strain amplitude. These findings provide compelling evidence for the injectable and self-healing properties of eutectogels. In order for a gel to be injectable, it must be able to restore its dynamic moduli after strain release and exhibit liquid-like flow under applied pressure. The observed thixotropic behavior confirms the injectability of the studied eutectogels.

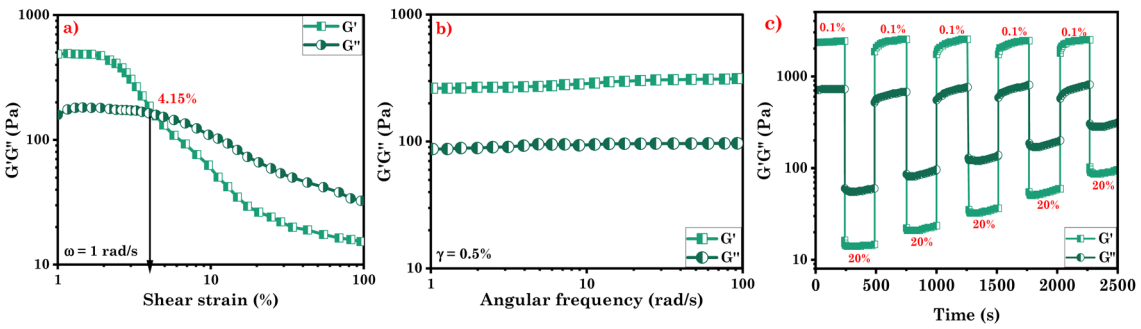

Fig. 5 (a) Strain sweep measurement (CG Gel); (b) frequency sweep measurement (CG Gel); and (c) thixotropic behavior (CG Gel).

Moreover, these findings also confirm the remarkable ability of the gels to self-heal and recover their original form without external stimuli (Video S2†).

3.4. Self-healing, adhesive and injectable properties of eutectogels

For a clearer insight, Fig. 6d provides a visual depiction showing the injectable characteristic of the eutectogel which is complemented by the depiction of its thixotropic behavior seen in Fig. 5c and S3c† (*vide supra*). When the strain applied to the eutectogel remains within the region of the compressed plunger of the injection (53 psi for the 10 mL syringe with 27-gauge needle),[54,55] the H-bonding network within the gel structure breaks down and it exhibits a fluid-like behavior, smoothly flowing from the needle. However, once the pressure is released, the gel swiftly reverts back to its original state (Video S2†). This reversible transformation showcases excellent adaptability, making it a promising material for various applications. The eutectogel exhibits a remarkable self-healing property, similar to biological tissues, where it can regenerate its noncovalent interactions after sustaining damage. To evaluate the self-healing ability of the eutectogel, it was divided into two fragments and dyed with two distinct dyes as shown in Fig. 6a. Subsequently, we intentionally brought the fragments into contact to assess their self-healing capacity. Remarkably, the eutectogel demonstrated self-healing along the cut line, as evidenced by the inverted microscopic image (Fig. 6b). In addition, we conducted a comprehensive investigation into the adhesive capabilities of the eutectogel with various surfaces. Our study encompassed glass, plastic, aluminum, and skin as substrates. The visual representation of our findings is shown in Fig. 6c, providing a concise depiction of the adhesive performance of the eutectogel across different surfaces. Furthermore, the lap shear displacement test was conducted to assess the strength of representative eutectogel (CG Gel) to adhere to various surfaces (*i.e.*, rubber, glass and skin) (Fig. S4†). A contact area of 15 mm was maintained between the eutectogel and the specific surface where the eutectogel was stretched at a regulated rate of 100 mm min^{-1} while the surface was fixed. The eutectogel showed highest adhesion on rubber (8.78 kPa) due to its flexibility, conforming to the surface. Adhesion on skin was slightly lower (8.11 kPa) due to variable mechanical properties of skin. On glass, adhesion was lowest (6.83 kPa) due to its rigid and smooth nature, limiting the contact area and adhesive strength.

3.5. *In vitro* biocompatibility assay

The drug delivery vehicle used in clinical applications must exhibit good biocompatibility to ensure it does not pose any risks or adverse effects. In the *in vitro* hemolysis assay, the DESs, ZIF-8, and eutectogels were discovered to be hemocompatible compared to the positive control (water). They exhibited minimal hemolysis, as evidenced by the results shown in Fig. 7a. The hemolysis % for CG DES, CF DES, ZIF-8, CG Gel, and CF Gel at a concentration of 10 mg mL^{-1} was found to be 0.85%, 0.76%, 0.90%, 0.98% and 0.92%, respectively. In contrast, the positive control (water) demonstrated complete hemolysis, with a hemolysis level of 100%. Hemolysis levels

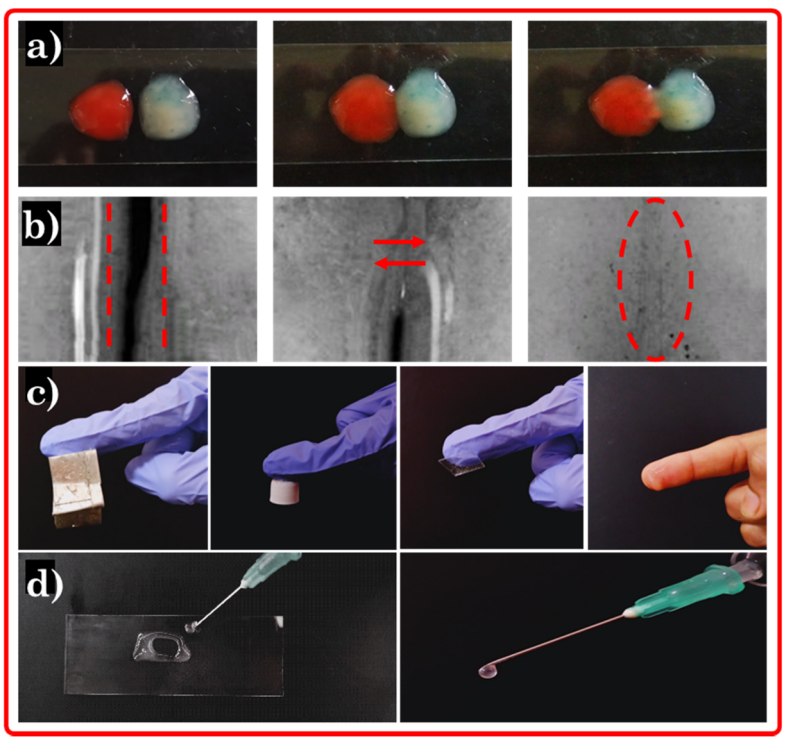

Fig. 6 (a) Visual image of self-healing, (b) inverted microscopic images of self-healing, (c) adhesive and, (d) injectable capability of the eutectogel.

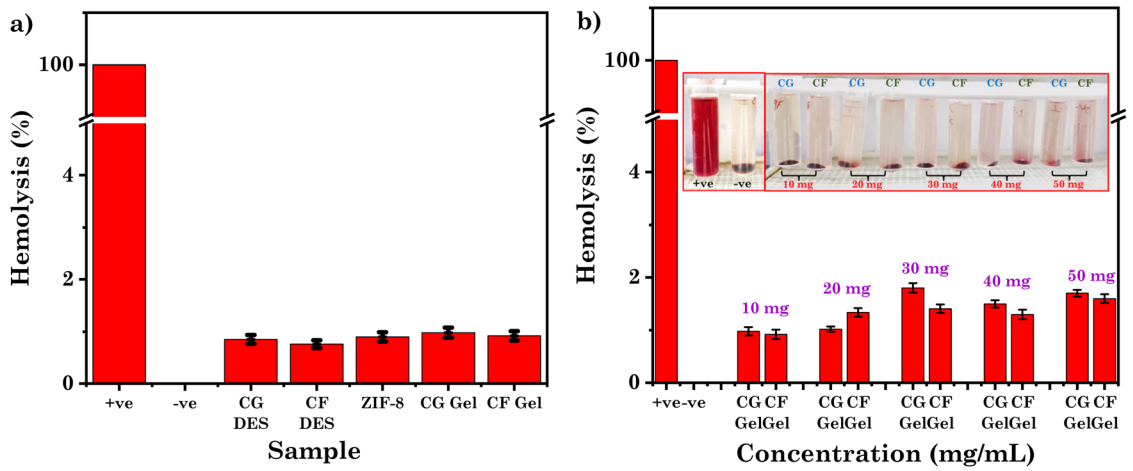

Fig. 7 (a) Hemolysis (%) level of CG/CF DES, ZIF-8 and CG/CF Gel; (b) hemolysis (%) level of CG/CF Gel at various concentrations.

below 5% are regarded non-toxic.[56] In our study, all samples showed less than 5% hemolysis across a range of increasing concentrations. Notably, eutectogels (CG and CF) exhibited minimal hemolysis even at high concentrations (50 mg mL^{-1}) as shown in Fig. 7b. Therefore, all eutectogel samples demonstrated high hemocompatibility. The hemolysis (%) level with increasing concentration of the eutectogel sample are summarized in Table S2.† ChCl, Glu, Fru, ZIF-8, and SA are all considered biocompatible materials which are used in the investigated system, suggesting that they are unlikely to induce adverse reactions or trigger immune responses upon contact with blood.[22,57–59] Furthermore, Glu and Fru are natural sugars commonly found in physiological solutions. Their presence in the eutectogel helps to maintain osmotic balance, thereby preventing hemolysis or disruption of RBCs when the gel comes into contact with blood components. ChCl, in addition to its biocompatibility, exhibits remarkable antithrombotic properties. It acts by inhibiting blood clot formation, thereby reducing the risk of thrombosis within the eutectogel. ChCl and natural sugar Fru based DES were used for the preparation of an ion gel, as reported in the literature. This ion gel has been demonstrated to be hemocompatible and oblivious to human RBCs.[22] While ChCl, Glu, and Fru play significant roles in ensuring the hemocompatibility of the eutectogel, the inclusion of ZIF-8 and SA offers additional functionalities. ZIF-8, provides structural integrity that enhances the drug loading property. SA, on the other hand, contributes to the biodegradability of the eutectogel and can facilitate controlled release of drugs.

Furthermore, the biocompatibility of the studied eutectogels was assessed using the human immortalised keratinocyte cell line (HaCaT). At a concentration of 15 mM, the biocompatibility assessment of the eutectogels showed a remarkable cell viability of about 94 and 93% for CG Gel and CF Gel, respectively (Fig. 8a and b). These findings strongly suggest the biocompatibility of the eutectogels, which makes them highly appealing for tissue engineering and drug delivery.

3.6. Drug loading and release profile in eutectogels

Their adhesive and injectable properties, coupled with biocompatibility, make eutectogels ideal for drug delivery applications. Consequently, we conducted a comprehensive investigation into the efficacy of incorporating curcumin, a potent medicinal compound, into the gel. Curcumin, derived from turmeric, is a natural compound with anti-inflammatory, antioxidant,[60] anticancer,[61] antimicrobial,[62] and neuroprotective properties.[63] It is promising towards treating various diseases like cancer, cardiovascular conditions,[64] neurodegenerative disorders,[65] arthritis,[63] and diabetes.[63] However, curcumin's clinical use is hindered by limitations including poor solubility and low bioavailability, which affect its delivery and effectiveness.[27] Another significant limitation of curcumin is its inherent instability, especially in water-based environments. It tends to degrade, compromising its desired concentration and activity.[27,66] This instability undermines its pharmaceutical effects and overall efficacy as a drug. Given the aforementioned limitations, it becomes imperative to investigate a suitable assembly that can effectively encapsulate curcumin, ensuring its stability within the delivery vehicle. To comprehend the potential of a eutectogel (CG Gel) as a drug delivery system, we investigated the stability of curcumin. Maintaining the pharmaceutical efficacy of curcumin requires understanding its time-dependent stability. Therefore, we stored curcumin-containing samples in a dark environment at room temperature within the CG Gel for a duration of 30 days. Remarkably, curcumin underwent only 38% degradation during this period (Fig. 9). In contrast, it takes only 24 hours for it to degrade by more than 90% when in water. Additionally, the absorbance maxima of curcumin did not exhibit any noticeable shifts, indicating the preserved molecular structure of the remaining curcumin. These findings contribute to our understanding of curcumin's stability within the CG Gel as a potential drug carrier.

To support this, we employed FTIR to assess the degradation behaviour of curcumin in both water and the represen-

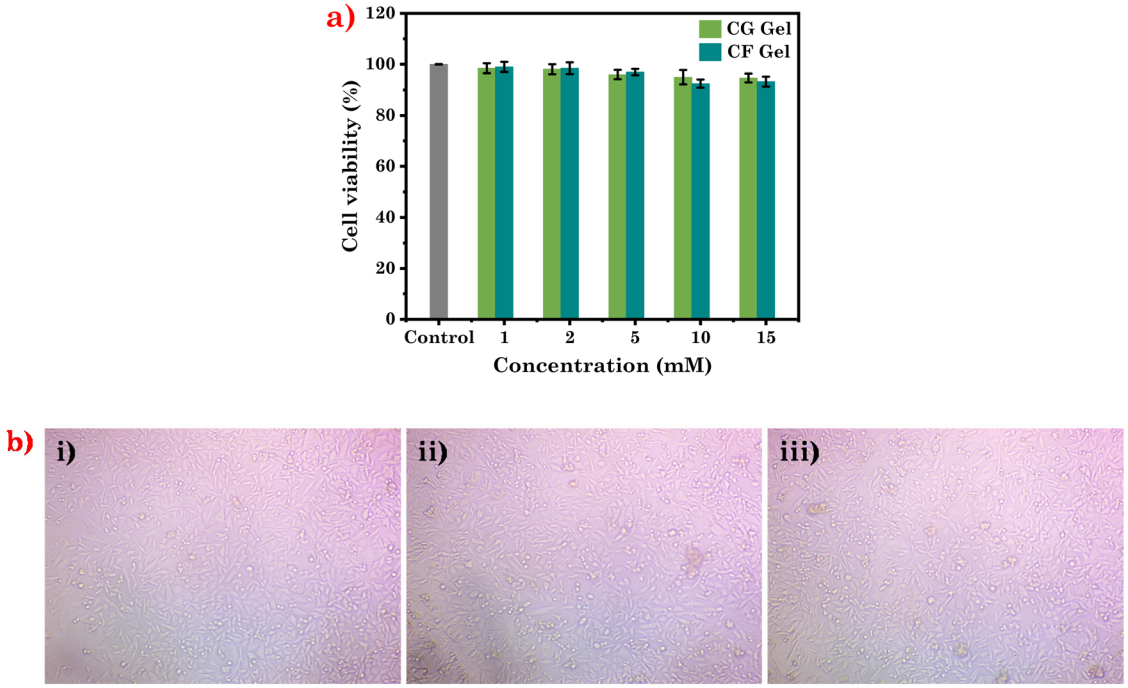

Fig. 8 (a) Cell viability (%) of HaCaT cells for CG and CF Gel; (b) Microscopic image of cytotoxicity on HaCaT cell (i) before treatment (control), (ii) after treatment with CG Gel and, (iii) after treatment with CF Gel after 48 h.

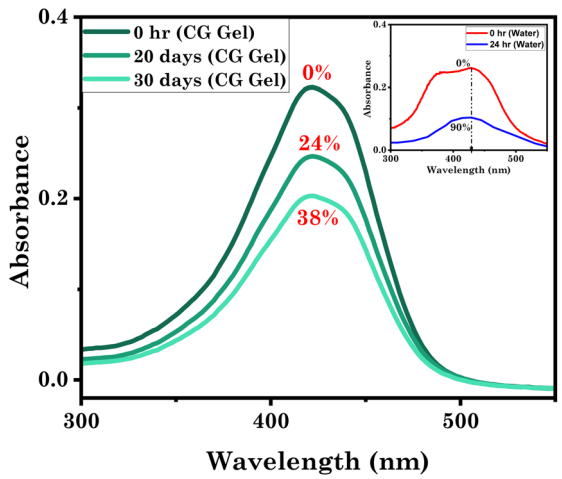

Fig. 9 Stability of curcumin within a representative eutectogel system studied by UV-Vis spectroscopy.

tative euetctogel (CG Gel). The comparative FTIR spectra of curcumin powder, curcumin in water at 0 hours, and curcumin in water at 24 hours are shown in Fig. S5a.† Curcumin exhibits specific bands at 3506 cm^{-1} (phenolic O–H stretching), 1624 cm^{-1} (aromatic C=C stretching), 1592 cm^{-1} (benzene ring stretching), 1504 cm^{-1} (C=O and C=C stretching), 1423 cm^{-1} (C–H bending), 1270 cm^{-1} (aromatic C–O stretching), and 1024 cm^{-1} (C–O–C stretching). These distinct vibrational bands of curcumin are present in the spectrum of curcumin dissolved in water at 0 hours. However, the intensity of these vibrational peaks is reduced, likely due to the low curcumin concentration in water because of its poor solubility in an aqueous environment. In contrast, these distinctive peaks are absent in the spectrum of curcumin in water after 24 hours, indicating that curcumin has undergone degradation during this period. Likewise, we examined the FTIR spectra of curcumin with CG Gel, both at the beginning (day 0) and after a 10-day period, as depicted in Fig. S5b.† The findings showed that even after 10 days, curcumin remained stable within the eutectogel.

We conducted further investigations to explore the effectiveness of the studied systems in loading curcumin. In CG Gel, curcumin exhibited an encapsulation of 45.60 mg g^{-1}, while in CF Gel, the encapsulation efficiency was 42.34 mg g^{-1}. Interestingly, the hydrophobic drug curcumin, which had an aqueous solubility of only 0.0006 mg mL^{-1}, showed a significant increase in solubility when encapsulated within the eutectogel. The enhanced curcumin encapsulation efficiency observed in the eutectogel can be attributed to the presence of ZIF-8 dispersed within the gel matrix. ZIF-8 possesses unique properties such as porosity and a high surface area.[30,42,43] These characteristics enable it to effectively load a greater amount of drug, curcumin. Additionally, the encapsulation within the eutectogel matrix further contributes to the improved encapsulation efficiency of curcumin. The combination of ZIF-8 and the eutectogel matrix creates a favorable environment for curcumin encapsulation, resulting in higher loading capacity and improved drug delivery potential.

Additionally, we conducted a comparative analysis of curcumin loaded eutectogel with other curcumin loaded systems (Table S3†), to gain valuable insights into the superior encapsulation efficiency and stability achieved by the studied eutectogels, highlighting its potential as an effective and reliable carrier for curcumin and other encapsulated drugs.

Furthermore, we conducted an investigation on the curcumin-loaded gel samples to assess their sustained release properties. Analysing the release profile of the drug enables controlled and programmed delivery, ensuring the drug is released over a specific duration. Drugs that undergo rapid metabolism can be quickly eliminated from the body after administration. However, by utilizing sustained release mechanisms or adjusting the rate of drug release, it becomes possible to maintain a constant concentration of the drug in the targeted organ. This is particularly beneficial for conditions like cancer, where a consistent dosage of the drug is not only advantageous but also cost-effective and safe. Considering these factors, we investigate the drug release potential of the eutectogel under physiological pH and temperature conditions. The release profile of curcumin from the CG Gel was examined, and the results revealed that approximately 64% of the encapsulated curcumin was released at pH 7.4. However, in acidic pH 5.0, a higher release of curcumin was observed, with approximately 86.5% being released. Similarly, in the CF Gel, the release of curcumin was investigated. At pH 7.4, approximately 67% of the curcumin was released from the gel matrix. However, when the pH was lowered to 5.0, a significantly higher release of curcumin was observed, with approximately 88% being released as shown in Fig. 10a and b. These findings indicate that the release of curcumin from both eutectogels is influenced by the pH of the surrounding environment. This can be attributed to the pH-responsive nature of ZIF-8, which allows for increased release under acidic conditions. The pH influence on the release behaviour of drug opens up possibilities for targeted and controlled drug delivery, particularly in applications where pH conditions vary, such as in certain disease environments.

To better understand the release of curcumin, we employed different kinetic models (as shown in Table S4†) to analyze its release behavior. These models aid in providing insights into the release kinetics of curcumin from the system under investigation. By comparing the data to different models, we found that the Higuchi Model provided the best fit for the curcumin release profile in both systems having higher r^2 value compared to other kinetic models (Fig. S6†). This model has been widely used to analyze and predict the release behavior of drugs from gel-based drug delivery systems.[67,68] It suggests that the drug release mechanism is primarily governed by diffusion. This diffusion-controlled release mechanism implies that the drug molecules are gradually released from the gel matrix as they diffuse through the gel structure, leading to a sustained and controlled release over time.

3.7. Antibacterial and antioxidant activities of eutectogels

The therapeutic benefits of curcumin are restricted due to its poor solubility in water. Nonetheless, our study has effectively shown that curcumin can be encapsulated at a high concentration (~45 mg g^{-1}) within the studied eutectogel samples, while maintaining its stability. Encouraged by these promising findings, our aim was to investigate the antibacterial activity of the studied systems. Table S5† summarizes the zone of inhibition as a measure of antibacterial activity for DESs and their corresponding gels, both with and without curcumin. Meanwhile, Fig. 11 provides visual representations of agar plates incubated for 18–20 hours at 37 °C. Upon examination of the image, it is evident that CG and CF DESs shows low to no zone of inhibition for both Gram-positive and Gram-negative bacterial strains. Likewise, our results agree with previously reported toxicological studies on this DES, specifically the ChCl : Glu DES. In the aforementioned studies, disc diffusion tests showed that ChCl : Glu DES had no harmful effects on a variety of microorganisms, including Gram-positive and Gram-negative bacteria.[69] Additionally, other research has shown that ChCl : glucose DES is a non-toxic solvent for a variety of microorganisms, such as fungi, Gram-positive and

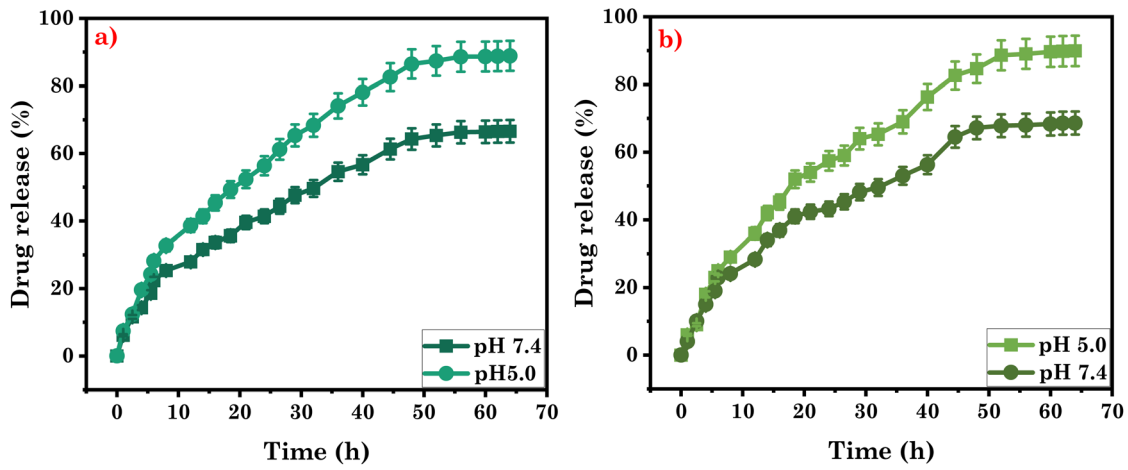

Fig. 10 Cumulative drug release (%) of (a) CG Gel and (b) CF Gel at pH 5.0 and 7.4.

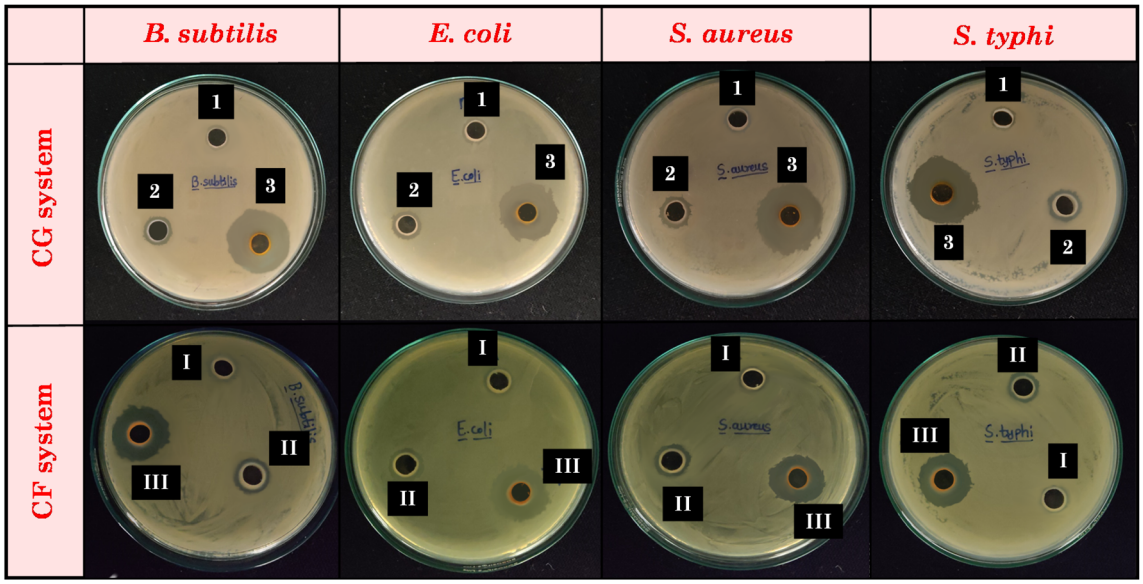

Fig. 11 Images showing zone of inhibition of pathogen cultured agar plates for both the systems. The numerical codes in the images are being used merely for the purpose of sample coding in each Petri dish. *i.e.*, (1) CG DES, (2) CG Gel, (3) CG Gel + Cur; (I) CF DES, (II) CF Gel, and (III) CF Gel + Cur.

Gram-negative bacteria.[70–72] Since, the DESs themselves show low to nil antibacterial activity, the gels derived from these DESs also did not exhibit significant antibacterial activity. On the other hand, we observed a notable increase in the antibacterial activity of the curcumin-loaded eutectogels compared to the pristine eutectogels (Fig. 12). This enhancement is due to the drug curcumin, which exhibits antibacterial activity against many microorganisms by rupturing the bacterial cell membranes. It affects both Gram-positive and Gram-negative bacteria by increasing membrane permeability, which ultimately leads to bacterial death.[73] The lipophilic nature of curcumin allows it to directly enter liposome bilayers, enhancing their permeability. Additionally, curcumin can disorder membranes and impact membrane fusion processes by inserting deeply into the membrane in a *trans*-bilayer orientation.[74] The membrane permeabilization characteristic of curcumin contributes to its direct antibacterial effect on both Gram-positive and Gram-negative bacteria.[75]

Curcumin also has potent antioxidant property, being able to scavenge free radicals and minimize oxidative stress. It protects cells from damage by inhibiting lipid peroxidation and scavenging reactive oxygen species (ROS) which are attributed to its chemical structure and its ability to donate hydrogen atoms or electrons to stabilize free radicals.[76] Here, the antioxidant activities of DESs and their gels, both with and without loaded curcumin, were evaluated using DPPH scaven-

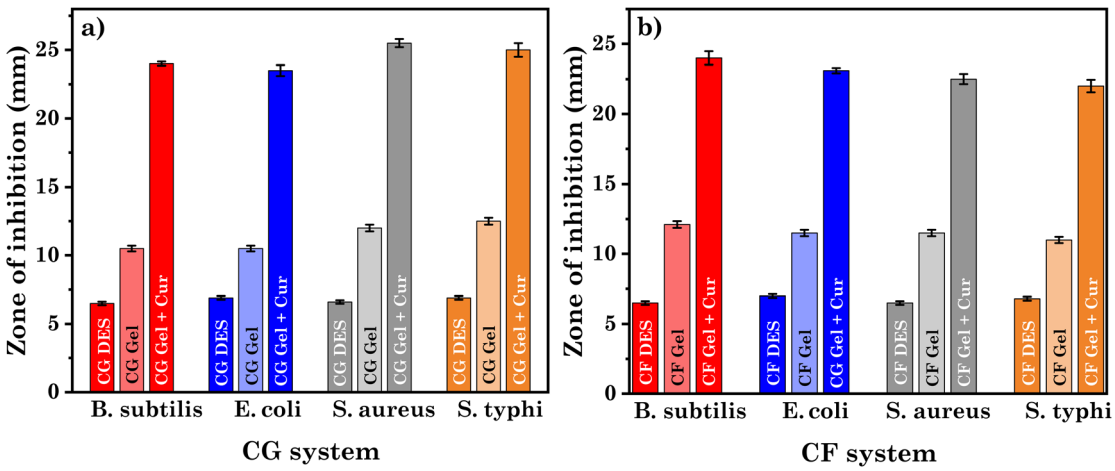

Fig. 12 Comparative representation of antimicrobial activities of DESs and their respective gel with and without curcumin CF system for (a) CG system and, (b) CF system.

Table 2 Percentage radical scavenging of all systems at different time intervals

Sample	Time (h)	(%) Inhibition	Sample	Time (h)	Inhibition (%)
CG Gel + Cur	4	22.43 ± 1.12	CF Gel + Cur	4	24.43 ± 1.22
	8	36.60 ± 1.83		8	39.69 ± 1.98
	16	45.68 ± 2.28		16	47.13 ± 1.35
	32	66.93 ± 2.34		32	69.84 ± 2.49
	48	83.74 ± 3.18		48	84.46 ± 2.22
CG DES	—	8.01 ± 0.40	CF DES	—	10.0 ± 0.50
CG Gel	—	9.20 ± 0.46	CF Gel	—	10.9 ± 0.54

ging activity. As demonstrated in Fig. S7b,† DESs (CG DES, CF DES) and gels (CG gel and CF gel) showed no significant antioxidant activities. However, curcumin loaded gels (CG Gel + Cur, CF Gel + Cur) demonstrated antioxidant activities reaching up to 83.7% and 84.4% respectively, as shown in Table 2. These enhancements were primarily achieved due to the potent antioxidant activity of curcumin.[77] Moreover, we carried out time-dependent DPPH scavenging activities of curcumin-loaded gels to investigate the antioxidant activity correlating to the release of the drug at different time intervals. Fig. S7a† shows increasing antioxidant activity over time, attributed to the sustained release of curcumin from the gel.

4. Conclusion

In summary, we successfully developed eutectogels by incorporating SA and ZIF-8 into DESs. The DESs and eutectogels were characterized by FTIR spectroscopy, and the structural integrity of ZIF-8 in the eutectogel was confirmed by XRD analysis. The dodecahedral shape of the synthesized ZIF-8 and the 3-D network of the eutectogel were assessed by SEM analysis. Using DSC, we determined the melting temperatures (T_m) to be 79 °C for CG Gel and 74 °C for CF Gel, which were further corroborated through visual observation and rheological experiments. The freezing temperature (T_f) was found to be −102 °C for CG Gel and −90 °C for CF Gel. Investigation into curcumin encapsulation showed remarkable loading capacities: 45.60 mg g^{-1} for CG Gel and 42.34 mg g^{-1} for CF Gel. When exposed to cancerous cell pH (5.0), both eutectogels showcased sustained release (64 h) of curcumin through diffusion, which was confirmed through the Higuchi model. The eutectogel exhibited excellent biocompatibility, with less than 2% hemolysis when in contact with human blood during *in vitro* hemolysis testing. When assessed for biocompatibility using the keratinocyte cell line (HaCaT), both eutectogels showed remarkable cell viability (94% for CG Gel and 93% for CF Gel), suggesting their excellent biocompatibility. Additionally, the curcumin-loaded eutectogels displayed potent antibacterial and antioxidant properties. This study holds promise in diverse fields, including environmental protection, advanced drug delivery, and tissue engineering. Their substantial curcumin loading and adhesive qualities make the eutectogels ideal for wound healing and localized drug delivery applications, while their thixotropic behavior suggests their potential as injectable drug delivery systems. Additionally, their anti-freezing property holds promise for treating conditions like frostbite in low-temperature environments, maintaining therapeutic effectiveness.

Author contributions

Nildhara Parsana: conceptualization, methodology, writing – original draft and visualization. Hiral Ukani: conceptualization, methodology, writing – original draft and visualization. Dharmveer Singh Chauhan: conceptualization, methodology, writing – original draft and visualization. Omar El Seoud: writing – original draft and visualization. Sanjay Mehra: conceptualization and methodology. Arvind Kumar: conceptualization and methodology. Naina Raje: conceptualization and methodology. Naved I. Malek: conceptualization, supervision, writing – review and editing, and funding acquisition. All authors have given their approval to the final version of the manuscript.

Conflicts of interest

There are no conflicts to declare.

Acknowledgements

NM acknowledges the financial assistance of UGC-DAE for the Collaborative Research Scheme (UDCSR/MUM/AO/CRS-M-997/2023). We also thank CNPq (grants 306108/2019-4; 141853/2019-0) and FAPESP (grant 2014/22136-4) for the grants to O. A. El Seoud.

References

1 S. J. Buwalda, T. Vermonden and W. E. Hennink, *Biomacromolecules*, 2017, **18**, 316–330.
2 J. Li and D. J. Mooney, *Nat. Rev. Mater.*, 2016, **1**, 16071.
3 H. Liu, W. Zhao, G. Gao and X. Ren, *Mater. Today Commun.*, 2019, **21**, 100609.
4 H. Gao, Z. Zhao, Y. Cai, J. Zhou, W. Hua, L. Chen, L. Wang, J. Zhang, D. Han, M. Liu and L. Jiang, *Nat. Commun.*, 2017, **8**, 15911.
5 G. D. Elliott, S. Wang and B. J. Fuller, *Cryobiology*, 2017, **76**, 74–91.
6 B. Zhang, J. Zhao, S. Chen, X. Zhang and W. Wei, *Int. J. Refrig.*, 2019, **99**, 176–185.
7 B. Zhang, H. Cao, H. Lin, S. Deng and H. Wu, *Food Chem.*, 2019, **278**, 482–490.
8 H.-Y. Wang, T. Inada, K. Funakoshi and S.-S. Lu, *Cryobiology*, 2009, **59**, 83–89.
9 B. B. Hansen, S. Spittle, B. Chen, D. Poe, Y. Zhang, J. M. Klein, A. Horton, L. Adhikari, T. Zelovich,

B. W. Doherty, B. Gurkan, E. J. Maginn, A. Ragauskas, M. Dadmun, T. A. Zawodzinski, G. A. Baker, M. E. Tuckerman, R. F. Savinell and J. R. Sangoro, *Chem. Rev.*, 2021, **121**, 1232–1285.
10 V. I. B. Castro, R. Craveiro, J. M. Silva, R. L. Reis, A. Paiva and A. R. C. Duarte, *Cryobiology*, 2018, **83**, 15–26.
11 A. R. Jesus, L. Meneses, A. R. C. Duarte and A. Paiva, *Cryobiology*, 2021, **101**, 95–104.
12 K. Hornberger, R. Li, A. R. C. Duarte and A. Hubel, *AIChE J.*, 2020, **67**, e17085.
13 S. J. Bryant, M. N. Awad, A. Elbourne, A. J. Christofferson, A. V. Martin, N. Meftahi, C. J. Drummond, T. L. Greaves and G. Bryant, *J. Mater. Chem. B*, 2022, **10**, 4546–4560.
14 E. L. Smith, A. P. Abbott and K. S. Ryder, *Chem. Rev.*, 2014, **114**, 11060–11082.
15 A. P. Abbott, D. Boothby, G. Capper, D. L. Davies and R. K. Rasheed, *J. Am. Chem. Soc.*, 2004, **126**, 9142–9147.
16 I. Wazeer, M. Hayyan and M. K. Hadj-Kali, *J. Chem. Technol. Biotechnol.*, 2018, **93**, 945–958.
17 J. Zhang, S. Li, L. Yao, Y. Yi, L. Shen, Z. Li and H. Qiu, *Chin. Chem. Lett.*, 2023, **34**, 107750.
18 K. Xin, I. Roghair, F. Gallucci and M. van Sint Annaland, *J. Mol. Liq.*, 2021, **325**, 115227.
19 Q. Zhang, K. De Oliveira Vigier, S. Royer and F. Jérôme, *Chem. Soc. Rev.*, 2012, **41**, 7108.
20 S. N. Pedro, M. S. M. Mendes, B. M. Neves, I. F. Almeida, P. Costa, I. Correia-Sá, C. Vilela, M. G. Freire, A. J. D. Silvestre and C. S. R. Freire, *Pharmaceutics*, 2022, **14**, 827.
21 M. Mokhtarpour, H. Shekaari and A. Shayanfar, *J. Drug Delivery Sci. Technol.*, 2020, **56**, 101512.
22 C. Mukesh, K. K. Upadhyay, R. V. Devkar, N. A. Chudasama, G. G. Raol and K. Prasad, *Macromol. Chem. Phys.*, 2016, **217**, 1899–1906.
23 Y. Guo, Y. Wang, H. Chen, W. Jiang, C. Zhu, S. Toufouki and S. Yao, *Carbohydr. Polym.*, 2022, **296**, 119939.
24 S. He, L. Wu, X. Li, H. Sun, T. Xiong, J. Liu, C. Huang, H. Xu, H. Sun, W. Chen, R. Gref and J. Zhang, *Acta Pharm. Sin. B*, 2021, **11**, 2362–2395.
25 M. R. Saeb, N. Rabiee, M. Mozafari and E. Mostafavi, *Materials*, 2021, **14**, 3652.
26 H. Ukani, Pratyush, S. Kumar, V. K. Aswal, A. A. Al-Ghamdi and N. I. Malek, *ChemistrySelect*, 2022, **7**, e202201613.
27 M. Jain, A. Marfatia, N. Imam, D. Ray, V. K. Aswal, N. Y. Patel, V. H. Raval, S. K. Kailasa and N. I. Malek, *J. Mol. Liq.*, 2021, **341**, 117396.
28 A. Shah, M. Kuddushi, S. Rajput, O. A. El Seoud and N. I. Malek, *ACS Omega*, 2018, **3**, 17751–17761.
29 R. Pansuriya, S. Mehra, A. Kumar, O. El Seoud, S. Kumar Kailasa and N. Malek, *J. Mol. Liq.*, 2023, **382**, 121857.
30 H. Ukani, S. Mehra, B. Parmar, A. Kumar, I. Khan, O. A. El Seoud and N. Malek, *Ind. Eng. Chem. Res.*, 2023, **62**, 5002–5014.
31 O. Frent, L. Vicas, N. Duteanu, C. Morgovan, T. Jurca, A. Pallag, M. Muresan, S. Filip, R.-L. Lucaciu and E. Marian, *Int. J. Mol. Sci.*, 2022, **23**, 12108.
32 S. Zhang, J. Dong, R. Pan, Z. Xu, M. Li and R. Zang, *Polymers*, 2023, **15**, 2149.
33 C. Huang, X. Chen, C. Wei, H. Wang and H. Gao, *Front. Pharmacol.*, 2021, **12**, 794939.
34 N. Parsana, S. Kumar, V. K. Aswal, O. El Seoud and N. I. Malek, *ACS Appl. Eng. Mater.*, 2023, **1**, 380–393.
35 P. Li, X. Cai, D. Wang, S. Chen, J. Yuan, L. Li and J. Shen, *Colloids Surf., B*, 2013, **110**, 327–332.
36 R. A. Moraes-de-Souza, T. L. C. Oldoni, M. A. B. Regitano-d'Arce and S. M. Alencar, *Cienc. Tecnol. Aliment*, 2008, **6**, 41–47.
37 H. N. Naik, D. Kanjariya, S. Parveen, A. Meena, I. Ahmad, H. Patel, R. Meena and S. Jauhari, *J. Biomol. Struct. Dyn.*, 2023, 1–13.
38 L. Sun, J. Han, C. Tang, J. Wu, S. Fang, Y. Li, Y. Mao, L. Wang and Y. Wang, *Cellulose*, 2022, **29**, 8133–8150.
39 Z. Belattmania, S. Kaidi, S. El Atouani, C. Katif, F. Bentiss, C. Jama, A. Reani, B. Sabour and V. Vasconcelos, *Molecules*, 2020, **25**, 4335.
40 H. Kaur, G. C. Mohanta, V. Gupta, D. Kukkar and S. Tyagi, *J. Drug Delivery Sci. Technol.*, 2017, **41**, 106–112.
41 T. Azizi Vahed, M. R. Naimi-Jamal and L. Panahi, *J. Drug Delivery Sci. Technol.*, 2019, **49**, 570–576.
42 Y. Song, N. Wang, L. Yang, Y. Wang, D. Yu and X. Ouyang, *Ind. Eng. Chem. Res.*, 2019, **58**, 6394–6401.
43 Q. Fu, S. Zhou, P. Wu, J. Hu, J. Lou, B. Du, C. Mo, W. Yan and J. Luo, *J. Solid State Chem.*, 2022, **307**, 122823.
44 Y. Tian, D.-W. Sun and Z. Zhu, *Food Chem.*, 2022, **371**, 131150.
45 J. Wang, Z. Ma, Y. Wang, J. Shao and L. Yan, *Macromol. Rapid Commun.*, 2021, **42**, 2000445.
46 P. Sun, J. Chen, Y. Li, X. Tang, H. Sun, G. Song, X. Mu, T. Zhang, X. Zha, F. Li, Y. Gao, S. Cong and Z. Zhao, *InfoMat*, 2023, **5**, e12363.
47 Y. Tian, D.-W. Sun, L. Xu, T.-H. Fan and Z. Zhu, *Food Hydrocolloids*, 2022, **128**, 107568.
48 S. Marullo, A. Meli, F. Giannici and F. D'Anna, *ACS Sustainable Chem. Eng.*, 2018, **6**, 12598–12602.
49 C. Zeng, H. Zhao, Z. Wan, Q. Xiao, H. Xia and S. Guo, *RSC Adv.*, 2020, **10**, 28376–28382.
50 J. Ruiz-Olles, P. Slavik, N. K. Whitelaw and D. K. Smith, *Angew. Chem., Int. Ed.*, 2019, **58**, 4173–4178.
51 L. Matthews, S. Ruscigno, S. E. Rogers, P. Bartlett, A. J. Johnson, R. Sochon and W. H. Briscoe, *Phys. Chem. Chem. Phys.*, 2021, **23**, 11672–11683.
52 M. Kuddushi, D. Ray, V. Aswal, C. Hoskins and N. Malek, *ACS Appl. Bio Mater.*, 2020, **3**, 4883–4894.
53 Y. Zheng, Y. Liang, D. Zhang, X. Sun, L. Liang, J. Li and Y.-N. Liu, *ACS Omega*, 2018, **3**, 4766–4775.
54 W. Hayward, L. Haseler, L. Kettwich, A. Michael, W. Sibbitt and A. Bankhurst, *Scand. J. Rheumatol.*, 2011, **40**, 379–382.
55 V. Pertici, C. Pin-Barre, C. Rivera, C. Pellegrino, J. Laurin, D. Gigmes and T. Trimaille, *Biomacromolecules*, 2019, **20**, 149–163.
56 H.-Y. Liu, L. Du, Y.-T. Zhao and W.-Q. Tian, *J. Nanomater.*, 2015, **2015**, 1–9.

57 L. Lomba, A. Polo, Á. Werner, C. Lafuente and B. Giner, *Eur. J. Pharm. Biopharm.*, 2023, **191**, 103–113.
58 L. R. de Moura Ferraz, A. É. G. A. Tabosa, D. D. S. da Silva Nascimento, A. S. Ferreira, V. de Albuquerque Wanderley Sales, J. Y. R. Silva, S. A. Júnior, L. A. Rolim, J. J. de Souza Pereira and P. J. Rolim-Neto, *Sci. Rep.*, 2020, **10**, 16815.
59 Z. Zou, B. Zhang, X. Nie, Y. Cheng, Z. Hu, M. Liao and S. Li, *RSC Adv.*, 2020, **10**, 39722–39730.
60 K. Jakubczyk, A. Drużga, J. Katarzyna and K. Skonieczna-Żydecka, *Antioxidants*, 2020, **9**, 1092.
61 M. Tomeh, R. Hadianamrei and X. Zhao, *Int. J. Mol. Sci.*, 2019, **20**, 1033.
62 Y.-S. Fu, T.-H. Chen, L. Weng, L. Huang, D. Lai and C.-F. Weng, *Biomed. Pharmacother.*, 2021, **141**, 111888.
63 L. Pari, D. Tewas and J. Eckel, *Arch. Physiol. Biochem.*, 2008, **114**, 127–149.
64 F. F. Cox, A. Misiou, A. Vierkant, N. Ale-Agha, M. Grandoch, J. Haendeler and J. Altschmied, *Cells*, 2022, **11**, 342.
65 S. Hu, P. Maiti, Q. Ma, X. Zuo, M. R. Jones, G. M. Cole and S. A. Frautschy, *Expert Rev. Neurother.*, 2015, **15**, 629–637.
66 R. W. Johnstone, *Nat. Rev. Drug Discovery*, 2002, **1**, 287–299.
67 V. A. Petrova, V. Y. Elokhovskiy, S. V. Raik, D. N. Poshina, D. P. Romanov and Y. A. Skorik, *Biomolecules*, 2019, **9**, 291.
68 M. Pradhan, K. Yadav, D. Singh and M. R. Singh, *J. Drug Delivery Sci. Technol.*, 2021, **61**, 102282.
69 M. Marchel, H. Cieśliński and G. Boczkaj, *Ind. Eng. Chem. Res.*, 2022, **61**, 11288–11300.
70 I. Juneidi, M. Hayyan and M. A. Hashim, *RSC Adv.*, 2015, **5**, 83636–83647.
71 B.-Y. Zhao, P. Xu, F.-X. Yang, H. Wu, M.-H. Zong and W.-Y. Lou, *ACS Sustainable Chem. Eng.*, 2015, **3**, 2746–2755.
72 Y. Huang, F. Feng, J. Jiang, Y. Qiao, T. Wu, J. Voglmeir and Z.-G. Chen, *Food Chem.*, 2017, **221**, 1400–1405.
73 G. K. Varshney, R. K. Saini, P. K. Gupta and K. Das, *Langmuir*, 2013, **29**, 2912–2918.
74 J. Barry, M. Fritz, J. R. Brender, P. E. S. Smith, D.-K. Lee and A. Ramamoorthy, *J. Am. Chem. Soc.*, 2009, **131**, 4490–4498.
75 P. Tyagi, M. Singh, H. Kumari, A. Kumari and K. Mukhopadhyay, *PLoS One*, 2015, **10**, e0121313.
76 M.-T. Huang, in *Food Factors for Cancer Prevention*, Springer, Japan, Tokyo, 1997, pp. 249–252.
77 C. Geng, X. Liu, J. Ma, H. Ban, H. Bian and G. Huang, *Carbohydr. Polym.*, 2023, **306**, 120612.